RSC Advances

PAPER

Cite this: *RSC Adv.*, 2023, **13**, 34410

Exploring the source of ammonia generation in electrochemical nitrogen reduction using niobium nitride†

So Young Park,[ac] So Eun Jang,[a] Chang Woo Kim,[b] Youn Jeong Jang*[c] and Duck Hyun Youn*[a]

Received 22nd September 2023
Accepted 17th November 2023

DOI: 10.1039/d3ra06475a

rsc.li/rsc-advances

In this study, niobium nitride (NbN) is prepared *via* the urea-glass route by annealing a mixture of $NbCl_5$ and urea at 650 °C under a flow of N_2, and is used as a catalyst for the electrochemical nitrogen reduction reaction (NRR). The as-prepared NbN exhibits a maximum production rate of 5.46×10^{-10} mol s^{-1} cm^{-2} at −0.6 V *vs.* RHE, along with an apparent FE of 16.33% at −0.3 V *vs.* RHE. In addition, the leaching of NbN is confirmed by ICP-OES, where the leached amount of Nb is almost identical to the amount of N measured by UV-vis. Moreover, ^{1}H NMR experiments are performed using $^{15}N_2$ as the feeder gas; the dominant detection of $^{14}NH_4^+$ peaks strongly suggests that the produced NH_3 originates from the leaching of NbN rather than *via* an electrocatalytic process. Hence, for a comprehensive understanding of NH_3 generation, especially when utilizing transition metal nitride (TMN)-based NRR catalysts, a thorough investigation employing multiple analytical methods is imperative.

Introduction

Ammonia (NH_3) is an indispensable material in various industrial fields, including fertilizers, explosives, pharmaceuticals, and plastics.[1,2] Moreover, due to its high hydrogen density of 17.6 wt%, along with its relatively high liquefaction point of −33.4 °C compared with that of hydrogen (−253 °C), increased attention has been focused on ammonia as an effective hydrogen carrier.[3,4] Currently, the Haber–Bosch (H–B) process is the dominant method for producing ammonia on an industrial scale. However, this process has significant drawbacks in terms of energy consumption (1% of the global total) and CO_2 emissions (1.67 tons per ton of NH_3), because it is operated at high temperatures (400–500 °C) and pressures (150–300 atm),[5,6] and because the necessary H_2 gas is mainly sourced from the steam methane reforming (SMR) of fossil fuels.[7–10] By contrast, the electrochemical nitrogen reduction reaction (NRR) can be operated under ambient conditions, and the requisite H_2 molecules are produced by water electrolysis powered by solar or wind energy,[11,12] thereby enabling a significant reduction in CO_2 emissions and energy consumption compared with the H–B process. Hence, the NRR is regarded as a promising approach for environmental-friendly production of ammonia.

In view of the above considerations, many studies and pioneering works have been conducted with the aim of developing efficient catalysts for the NRR. However, the NRR performance is generally compromised by the competing hydrogen evolution reaction (HER), which involves only two electrons and requires a lower overpotential than the NRR.[13,14] Consequently, the NH_3 production rates and faradaic efficiencies (FE) of the presently-available NRR catalysts remain far below the target set by the practical utilization guidelines of the United States Department of Energy (US DOE), which call for a current density 300 mA cm^{-2} and an FE of 90%.[15,16] Therefore, to enhance the NRR activity of the catalyst, it is necessary to develop a catalyst that can reduce its HER performance by reducing its affinity for hydrogen and increasing its affinity for nitrogen.

Among the various catalysts, transition metal nitrides (TMNs) are regarded as particularly promising catalysts for the NRR due to their unique Mars–van Krevelen (MvK) mechanism.[16,17] Indeed, density functional theory (DFT) studies have suggested that TMNs can effectively lower the HER, thereby potentially providing enhanced NRR activities.[18–22] In particular, VN, CrN, NbN, and ZrN have been suggested as promising candidates for the NRR. Inspired by DFT results, various TMNs were employed for NRR. However, recent studies on the TMNs and their ability to produce ammonia have suggested two different opinions, namely: (1) catalytic reaction *via* the MvK mechanism (or others), and (2) non-catalytic reaction *via* leaching or decomposition of the catalyst. For instance, Zhang *et al.* reported that VN loaded on carbon cloth (VN/CC) catalyst yielded NH_3 at a rate of 2.48×10^{-10} mol s^{-1}

[a]*Department of Chemical Engineering, Department of Integrative Engineering for Hydrogen Safety, Kangwon National University, Chuncheon 24341, South Korea. E-mail: youndh@kangwon.ac.kr*

[b]*Department of Nanotechnology Engineering, Pukyong National University, Busan 48513, South Korea*

[c]*Department of Chemical Engineering, Hanyang University, Seoul 04763, South Korea. E-mail: yjang53@hanyang.ac.kr*

† Electronic supplementary information (ESI) available. See DOI: https://doi.org/10.1039/d3ra06475a

cm^{-2} with an FE of 3.58%,[23] thereby indicating catalytic activity, whereas Du *et al.* reported that VN displayed non-catalytic activity, and produced NH_3 *via* the reduction of the released lattice N^{3-} atoms.[24] Similarly, Mo_2N has been investigated by two different groups, with one group reporting an NH_3 yield of 78.4 μg h^{-1} mg^{-1}_{cat} with an FE of 4.5% *via* a catalytic mechanism,[25] while the second group reported a maximum FE of 42.3% at −0.05 V *vs.* RHE and a yield of 2.73 μg h^{-1} mg^{-1} at 0.05 V, due to Mo_2N decomposition.[26] The latter conclusion was evidenced by the ^1H NMR spectra, which exhibited only $^{14}NH_4^+$ peaks despite the use of $^{15}N_2$ as the feeder gas. The other studies concerning the leaching or decomposition of TMN-based catalysts are summarized in Table S1.† Meanwhile, NbN catalysts are expected to have catalytic activity for NRR owing to the N-vacancy regeneration and durability of the catalytic cycle on NbN (111) facet based on previous DFT investigations.[27] Nevertheless, experimental studies on the use of NbN as an NRR catalyst are rare.

Hence, in the present study, an NbN catalyst is prepared by a simple urea glass route, and its NRR performance in alkaline solution is investigated thoroughly in order to determine the origin of the produced ammonia. The as-prepared NbN exhibits an NH_3 yield of 5.46×10^{-10} mol s^{-1} cm^{-2} at −0.6 V *vs.* RHE, and an apparent FE of 16.33% at −0.3 V *vs.* RHE. By combining inductively coupled plasma optical emission spectrometry (ICP-OES), ultraviolet-visible spectrophotometer (UV-vis) and isotope nuclear magnetic resonance (NMR) characterization, the produced ammonia is proven to be generated by leaching of the catalyst, with mainly $^{14}NH_4^+$ peaks being detected in the NMR spectrum despite the use of $^{15}N_2$ as the feeder gas. Moreover, the amount of leached Nb measured by ICP-OES is almost identical to the amount of N detected by UV-vis. Thus, the present study strongly demonstrates that the produced NH_3 originates from leaching of the NbN, and is expected to provide a good guideline for the selection of catalysts for the NRR.

Materials and methods

Materials

Niobium(v) chloride ($NbCl_5$; 99%), ammonium chloride (NH_4Cl; ≥99.5%), 4-(dimethylamino)benzaldehyde (*p*-$C_9H_{11}NO$; ≥99%), dimethyl sulfoxide-d_6 (DMSO-d_6; 99.9 atom% D), $^{15}N_2$ (98 atom% ^{15}N), ammonium-^{15}N chloride ($^{15}NH_4Cl$; ≥98 atom% ^{15}N), potassium sodium tartrate tetrahydrate ($KNaC_4H_4O_6$; 99%), and graphite rods (99.995% trace metals basis) were purchased from Sigma-Aldrich. N_2 (high purity, 99.999%) and Ar (high purity, 99.999%) gases were purchased from Hyundai energy. Urea (99.0%), ethyl alcohol (C_2H_5OH; 99.9%, anhydrous), and hydrochloric acid (HCl; 35.0–37.0%) were purchased from Samchun Chemicals. Hydrazine monohydrate ($N_2H_4 \cdot H_2O$; 98+%) was obtained from Alfa-Aesar, Nessler solution was obtained from Fischer Chemical, and carbon paper (CP; AvCarb MGL 370) was purchased from Fuel Cell store.

NbN synthesis

NbN was synthesized *via* the urea-glass route.[28] In a typical synthesis, 1000 mg of $NbCl_5$ was dispersed in 2.53 ml of ethanol, and 1509 mg of urea was added to the solution under magnetic stirring. After stirring for 1 h, the resultant viscous solution was transferred into an alumina boat and annealed at 650 °C for 3 h under a flow of N_2. Before removing the alumina boat from the furnace at room temperature, mixed N_2/air gas was allowed to flow for 10 min to prevent rapid oxidation of the NbN (passivation).

Characterization

The crystalline structure of the catalyst was analyzed by X-ray diffraction (XRD; Rigaku, MiniFlex 600) with Cu-Kα ($\lambda = 1.54$ Å) radiation. The surface morphologies were investigated using a field-emission scanning electron microscope (FE-SEM; JEOL, JMS-7000F) equipped with an energy dispersive spectrometer (EDS). X-ray photoelectron spectroscopy (XPS; Thermo Scientific, K alpha) was used to characterize the surface oxidation states and chemical compositions. The produced ammonia was detected by UV-vis spectrophotometer (UV-vis; SHIMADZU, UV-2600i) and the leached metal was quantified *via* inductively coupled plasma optical emission spectrometer (ICP-OES; Agilent, Agilent 5900).

Electrochemical measurements

A potentiostat (AMETEK, VersaSTAT 3) was used to conduct the electrochemical measurements in a single-compartment cell equipped with a three-electrode system, and a 0.1 M KOH solution served as the electrolyte (Fig. S1†). The working electrode, designated as NbN/CP, was prepared by dispersing 10 mg of the NbN catalyst in 500 μL of ethanol and then loading it onto 1×1 cm^2 carbon paper (with a mass loading of 2 mg cm^{-2}) by drop casting. A graphite rod and Ag/AgCl (3 M NaCl) were used as the counter and reference electrode, respectively. All recorded potentials were converted to reversible hydrogen electrode (RHE). Linear sweep voltammetry (LSV) was conducted at a scan rate of 5 mV s^{-1} and chronoamperometry tests were performed for 2 h at −0.3 to −0.6 V *vs.* RHE. Prior to the LSV test, cyclic voltammetry (CV) was performed at a scan rate of 50 mV s^{-1} for 20 cycles in order to stabilize the catalyst. The electrolyte was continuously bubbled with N_2 gas for 30 min prior to and throughout the duration of these tests.

Ammonia detection

The amounts of produced NH_3 in the electrolyte and in the acid trap after electrolysis were detected *via* Nessler's method.[29] The acid trap, connected to the gas-out line of the reaction cell (Fig. S1†), was employed to capture NH_3 that escaped without dissolving in the electrolyte during the reaction. 0.05 M H_2SO_4 was utilized for this purpose. In this approach, 5 ml of each aliquot from each source was mixed with 0.1 ml of 500 g L^{-1} $KNaC_4H_4O_6$ and 0.1 ml of Nessler's solution and incubated for 20 min at room temperature. The absorbance of the mixed solution was then analyzed at 420 nm. The absorbance concentration (abs–conc) plots were calibrated against standard NH_4Cl solutions with concentrations of 0, 0.5, 1.0, 2.0, 3.0, 4.0, and 5.0 μg ml^{-1} in 0.1 M KOH (Fig. S2a of the ESI†), and the calibration curve showed $y = 0.1419x - 0.0017$ ($r^2 = 0.99996$)

(Fig. S2b†). In addition, the abs–conc plots of the aliquots from the acid trap solution were calibrated against standard NH_4Cl solutions with concentrations of 0, 0.1, 0.2, 0.5, 1.0, and 2.0 μg ml^{-1} in 0.05 M H_2SO_4 (Fig. S2c†), and the calibration curve was $y = 0.1851x - 0.0005$ ($r^2 = 0.99892$) with a good linear relationship (Fig. S2d†). The pH of the acid trap solution was adjusted to ~13 by the addition of 1 M KOH solution.[30]

Hydrazine detection

The Watt and Chrisp method was used to test for the presence of N_2H_4, which is a potential by-product of the NRR.[31] First, the detection reagent was prepared by adding 5.99 g of *p*-$C_9H_{11}NO$ to 30 ml of HCl and 300 ml of C_2H_5OH. After collecting 5 ml of electrolyte from the electrolytic cell, 5 ml of the reagent was added and the resulting mixture was allowed to stand for 10 min prior to measurement of the absorbance at 455 nm. The abs–conc plots were calibrated against standard $N_2H_4 \cdot H_2O$ solutions with concentrations of 0, 0.2, 0.4, 0.6, 0.8, 1.0 μg ml^{-1} in 0.1 M KOH (Fig. S3a†), and the fitted curve was $y = 0.7401x + 0.1140$ ($r^2 = 0.99984$) (Fig. S3b†).

$^{15}N_2$ isotope test and NMR analysis

To determine whether ammonia was produced from the N_2 feeder gas, the $^{15}N_2$ isotopic test was conducted and the $^{15}NH_4^+$ was analyzed by proton nuclear magnetic resonance spectrometer (^{1}H NMR; Bruker, Bruker Avance Neo 600) with 600 MHz. After 2 h of chronoamperometry (Ammonia detection section), 20 ml of the electrolyte was acidified to pH 2 by addition to concentrated HCl (20 μl), and then concentrated to 2–3 ml *via* rotary evaporator. Next, 950 μl of the condensed solution was mixed with 50 μl of DMSO-d_6, and 600 μl of the resulting mixture was transferred to an NMR tube.[32] For comparison, the 0.1 M KOH solution, the $^{14}NH_4Cl$ standard, the $^{15}NH_4Cl$ standard, and a sample obtained after chronoamperometry using $^{14}N_2$ as the feeder gas were also analyzed. The spectrum of each sample was obtained using 1024 scans with an acquisition time of 3 s and a relaxation delay of 1.5 s.[33]

Calculation of production rates and faradaic efficiency (FE)

The ammonia production rate (r) and faradaic efficiency (FE) were calculated by using eqn (1) and (2), respectively:

$$r = \frac{C_{NH_3} \times V}{m_{NH_3} \times t \times A} \quad (1)$$

$$FE = \frac{n \times F \times C_{NH_3} \times V}{m_{NH_3} \times Q} \quad (2)$$

where C_{NH_3} is the measured concentration (in μg ml^{-1}) of ammonia, V is the volume (in L) of the electrolyte, m_{NH_3} is the molar weight of ammonia (17.031 g mol^{-1}), t is the reaction time (in s), A is the electrode area (cm^2), F is faradaic constant (96 485C mol^{-1}), Q is the passed charge during electrolysis, and n is the number of electrons needed to produce ammonia (*i.e.*, 3).

Results and discussion

The physical properties of the NbN catalyst

The XRD pattern of the as-prepared NbN catalyst is presented in Fig. 1a, where the observed peaks at 35.5°, 41.2°, 59.7°, 71.4°, and 75.1° are assigned to the respective 111, 200, 220, 311, and 222 planes, corresponding to the reference pattern for cubic NbN (JCPDS 03-065-9399). The broad peak at around 20–30° is due to residual carbon from the urea,[34] while peaks due to other potential impurities such as niobium metal or niobium oxides are not observed. The particle size of the catalyst was calculated to be about 5 nm according to the Debye–Scherrer equation. For comparison, the XRD pattern of the NbN without passivation is provided in Fig. S4,† where intense Nb_2O_5 peaks are observed along with those of NbN, and the unpassivated sample is seen to be oxidized and has developed a white coloration (lower inset). These results demonstrate that passivation can prevent the formation of the crystalline Nb_2O_5 phase, thereby resulting in the formation of crystalline NbN with an amorphous oxide layer.

The surface chemical composition and oxidation state of the NbN catalyst are revealed by the XPS results in Fig. 1b–d. Here, the survey spectrum indicates the presence of the elements Nb, N, C, and O elements (Fig. 1b). Moreover, the high-resolution Nb 3d spectrum can be deconvoluted into three pairs of peaks, corresponding to NbN (204.4 and 206.8 eV), NbON (205.6 and 208.5 eV), and Nb_2O_5 (207.3 and 209.8 eV), respectively (Fig. 1c).[35–38] Here, the oxidized species, NbON and Nb_2O_5, are due to the passivation step and the inevitable oxidation upon exposure to air. Meanwhile, the N 1s spectrum in Fig. 1d exhibits two deconvoluted peaks at 397.17 and 399.6 eV due to NbN and NbON, respectively.[35,39,40]

The NbN catalyst is further characterized by the SEM image in Fig. 2a, where the NbN particles form clusters with sizes of ~50 μm. In addition, the high-resolution SEM image and

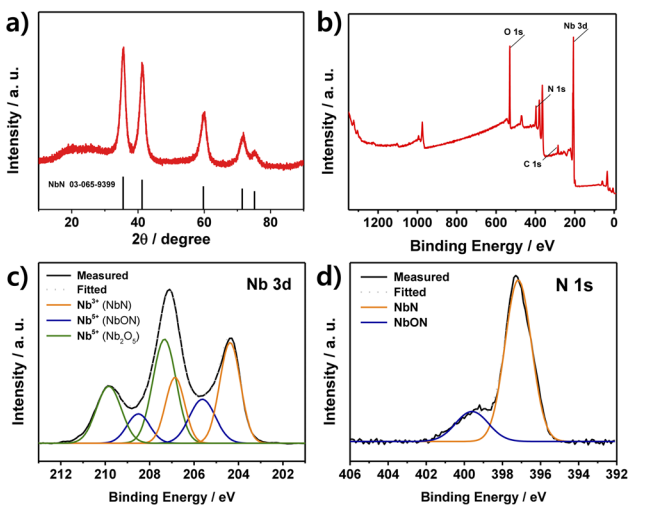

Fig. 1 (a) The XRD pattern of the as-synthesized NbN. (b–d) The XPS analysis of the as-synthesized NbN, including (b) the full survey scan, (c) the high-resolution Nb 3d spectrum, and (d) the high-resolution N 1s spectrum.

corresponding elemental mapping images in Fig. 2b reveal almost identical distributions of Nb, N, and O, thereby indicating the generation of NbN with surface oxidized species.

The electrochemical properties of the NbN on a carbon paper electrode

The LSV curves of the NbN/CP electrode in N_2- and Ar-saturated 0.1 M KOH solutions are presented in Fig. 3a. Here, the N_2-saturated solution (red profile) exhibits a slightly higher current density than does the Ar-saturated solution (black profile) below −0.3 V. Therefore, the chronoamperometry (CA) tests in Fig. 3b were conducted in the range of −0.3 to −0.6 V for 2 h, during which a stable current density was observed at each applied potential, and the current density was seen to increase with the increase in applied potential. Further, the average production rates and apparent FEs calculated after the 2 h CA tests are presented in Fig. 3c, where the apparent FE is seen to decrease gradually from a maximum of 16.33% at −0.3 V to 1.32% at −0.6 V. This is because the competitive HER becomes dominant at the more negative potentials.[23,25,34,41] However, the measured production rates are fairly similar at each potential (with a maximum of 5.46×10^{-10} mol s^{-1} cm^{-2} at −0.6 V), thus suggesting that the detected NH_3 might not have originated from the NRR. Hence, the NH_3 production rates under various control conditions are presented in Fig. 3d.

Here, near-zero NH_3 production rates are observed for both the 0.1 M KOH and the bare CP (without any catalyst), thereby demonstrating that these components do not contribute to the production of ammonia in the presence of NbN/CP. Meanwhile, in the presence of the NbN/CP electrode, the similar NH_3 production rate of 5.32×10^{-10} mol s^{-1} cm^{-2} is observed in the N_2-saturated solution and that of 4.56×10^{-10} mol s^{-1} cm^{-2} in the Ar-saturated solution after 2 h at −0.6 V. Moreover, the NbN/CP produces a similarly low amount of ammonia (4.3×10^{-10} mol s^{-1} cm^{-2}) even in the N_2-saturated solution when open circuit potential (OCP) conditions are used. Generally, TMN-based catalysts can generate ammonia *via* the leaching and subsequent reduction of surface N atoms under N_2-saturated solution. This leaves surface N-vacancies that can become occupied by N_2 molecules, thereby proceeding the catalytic reaction. Meanwhile, under Ar-saturated solution, ammonia can only be generated *via* leaching and the surface N-vacancies

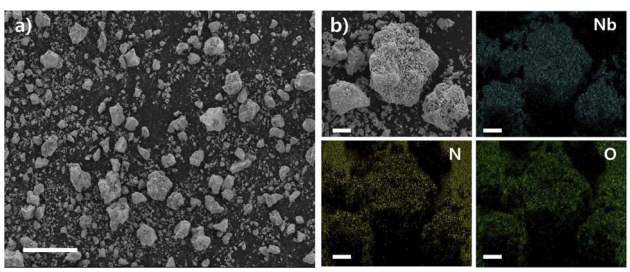

Fig. 2 (a) A SEM image of the as-synthesized NbN. (Scale bar = 100 μm) (b) a high-resolution SEM image and the corresponding EDS elemental mapping images of Nb, N and O. (Scale bar = 10 μm).

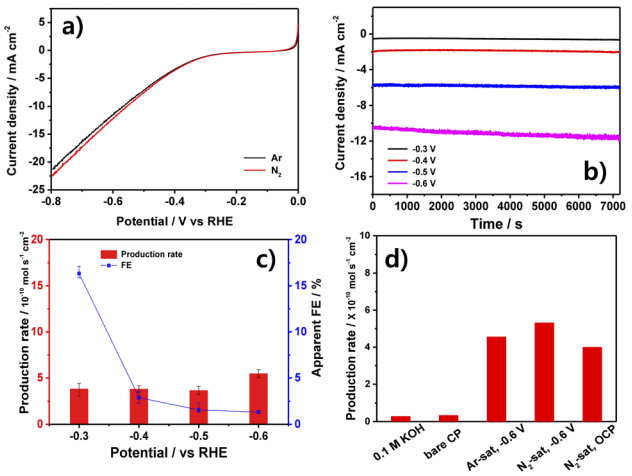

Fig. 3 The electrochemical characterization of the NbN catalyst in 0.1 M KOH solution: (a) the LSV curves obtained in N_2- and Ar-saturated solutions, (b) the 2 h chronoamperometry profiles at various applied potentials, (c) the NH_3 production rates and apparent FEs at various potentials after 2 h of electrolysis, and (d) the NH_3 production rates of the following control samples: (i) the 0.1 M KOH, (ii) the 0.1 M KOH after chronoamperometry using the bare CP as the working electrode, (iii) an Ar-saturated solution after chronoamperometry using the NbN/CP as working electrode at −0.6 V, (iv) an N_2-saturated solution after chronoamperometry using the NbN/CP as working electrode at −0.6 V, and (v) an N_2-saturated solution after chronoamperometry using the NbN/CP as working electrode at OCP.

can't be replenished by N_2 molecules, thereby preventing the catalytic reaction. Therefore, a much lower amount of ammonia is produced in Ar-saturated solutions than in N_2-saturated solutions.[25,42] Hence, the present results strongly suggest that the produced ammonia does not originate from the NRR, and is likely to be the result of catalyst leaching. In the following hydrazine detection experiment in Fig. S5,† no hydrazine was detected, eliminating the possibility for by-product generation. Hence, the non-electrochemical origin of the produced ammonia is further investigated in the following section.

The origin of produced ammonia

The leaching of the catalyst is revealed by monitoring the Nb concentration *via* ICP-OES while simultaneously monitoring the concentration of N (in form of NH_3) *via* UV-vis spectroscopy.[43] The results are presented in Fig. 4 and summarized in Table S2.† Thus, in the potential range of −0.3 to −0.6 V (including OCP), the measured concentrations of Nb and N are quite similar, and the Nb/N molar ratio is close to 1. These results strongly support the hypothesis that the NbN catalyst leaches into the electrolyte, and that the N of the leached NbN is responsible for the produced ammonia.[24]

To further confirm the origin of the produced ammonia, the ^1H NMR spectra of the 0.1 M KOH, the $^{14}NH_4Cl$ and $^{15}NH_4Cl$ standards (each dissolved in 0.1 M KOH), and the electrolyte samples collected after 2 h of chronoamperometry in the presence of the NbN/CP using $^{14}N_2$ and $^{15}N_2$ as the feeder gas are presented in Fig. 5. Here, no peaks are detected for the 0.1 M KOH (black line, Fig. 5), thereby indicating that the electrolyte

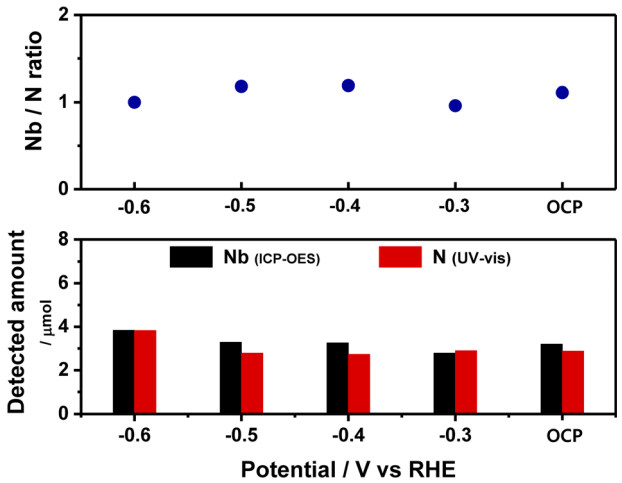

Fig. 4 The Nb/N ratio (top) and the detected amounts of Nb and N atoms (bottom).

itself does not contribute to the production of ammonia. Meanwhile, the standard $^{14}NH_4Cl$ (red line) and $^{15}NH_4Cl$ (blue line) solutions in 0.1 M KOH exhibit the characteristic triplet peaks of $^{14}NH_4^+$ and doublet peaks of $^{15}NH_4^+$, respectively. Moreover, when $^{14}N_2$ is employed as the feeder gas in the presence of the catalyst, only the $^{14}NH_4^+$ triplet is observed, as expected (pink line). However, when $^{15}N_2$ is used as the feeder gas (green line), the $^{14}NH_4^+$ triplet is again observed, along with a negligible $^{15}NH_4^+$ doublet. This confirms that the produced NH_3 does not originate from the electrocatalytic reaction.

Based on the above ICP-OES and NMR results, it is concluded that the NbN is leached out to the electrolyte, and that the leached N atoms are reduced to ammonia ions. Therefore, the ammonia produced using NbN/CP is primarily a result of the non-electrocatalytic reaction (the nitride leaching process). Based on the results presented earlier, the FE calculated using eqn (2) as depicted in Fig. 3 lacks significance due to the non-electrochemical nature of our process. FE is traditionally expressed as the ratio of the charge applied to generate the target product to the total charge passed during the reaction. According to this definition, the product should receive electrons through the charge applied. However, given that the production of ammonia is not exclusively a result of the passed charge, our findings are not well-suited for the use of FE, a metric commonly employed in electrochemical reactions. Therefore, we wrote it as 'apparent FE', instead of FE (Fig. 3c). In light of this, researchers interested in employing TMN-based catalysts should exercise caution. As we have elucidated earlier, ammonia can be generated through the leaching or decomposition of the catalyst itself. Therefore, it is crucial to determine whether this process qualifies as an electrochemical reaction or a chemical reaction by employing multiple analytical techniques such as ICP-OES and NMR using $^{15}N_2$ isotope.

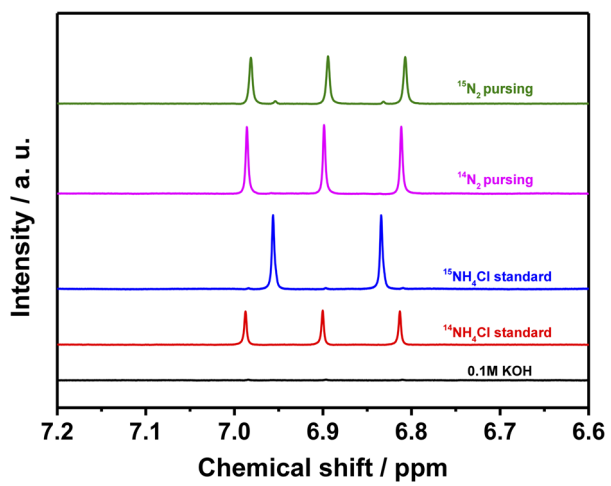

Fig. 5 The ^1H NMR spectra of the 0.1 M KOH solution, the $^{14}NH_4Cl$ standard, the $^{15}NH_4Cl$ standard, and the electrolyte samples collected after 2 h of chronoamperometry in the presence of the NbN/CP using $^{14}N_2$ and $^{15}N_2$ as the feeder gas.

Conclusions

Herein, a niobium nitride (NbN) for the electrochemical nitrogen reduction reaction (NRR) was prepared *via* the urea-glass route by annealing a mixture of niobium(v) chloride ($NbCl_5$) and urea. An electrode consisting of the as-synthesized NbN on carbon paper (NbN/CP) exhibited an NH_3 yield of 5.46 $\times$ 10^{-10} mol s^{-1} cm^{-2} at -0.6 V, with an apparent faradaic efficiency (FE) of 16.33% at -0.3 V. However, the results of inductively coupled plasma optical emission spectrometry (ICP-OES) indicated leaching of the NbN, with the leached amount of Nb closely matching the amount of N measured by ultraviolet-visible (UV-vis) spectroscopy. Moreover, this conclusion was further supported by the dominant detection of $^{14}NH_4^+$ peaks in proton nuclear magnetic resonance (^1H NMR) experiments using $^{15}N_2$ as the feeder gas. Therefore, it is crucial to thoroughly investigate the origin of NH_3 in transition metal nitride (TMN)-based catalysts for the NRR, and the approach used in the present study is expected to provide a good guideline for selecting suitable catalysts for NRR.

Conflicts of interest

The authors declare that they have no known competing financial interests or personal relationships that could have appeared to influence the work reported in this paper.

Acknowledgements

This study was supported by the National Research Foundation of Korea (NRF) grant funded by the Korea government (Ministry of Education) (2019R1I1A3A01052741) and Quantum Simulator Development Project for Materials Innovation through the NRF funded by the Korea government (Ministry of Science and ICT, MSIT) (No. NRF-2023M3K5A1094813). This work was also supported by the Korea Institute of Energy Technology Evaluation and Planning (KETEP) and the Ministry of Trade, Industry & Energy (MOTIE) of the Republic of Korea (No. 20224000000080).

The Korea Basic Science Institute (Chuncheon) provided assistance with the SEM analyses.

Notes and references

1 G. Qing, R. Ghazfar, S. T. Jackowski, F. Habibzadeh, M. M. Ashtiani, C.-P. Chen, M. R. Smith III and T. W. Hamann, *Chem. Rev.*, 2020, **120**, 5437–5516.

2 A. Afif, N. Radenahmad, Q. Cheok, S. Shams, J. H. Kim and A. K. Azad, *Renewable Sustainable Energy Rev.*, 2016, **60**, 822–835.

3 S. Ghavam, M. Vahdati, I. A. G. Wilson and P. Styring, *Front. Energy Res.*, 2021, **9**, 580808.

4 B. Yang, W. Ding, H. Zhang and S. Zhang, *Energy Environ. Sci.*, 2021, **14**, 672–687.

5 N. Cao and G. Zheng, *Nano Res.*, 2018, **11**, 2992–3008.

6 X. Guo, H. Du, F. Qu and J. Li, *J. Mater. Chem. A*, 2019, **7**, 3531–3543.

7 C. Smith, A. K. Hill and L. Torrente-Murciano, *Energy Environ. Sci.*, 2020, **13**, 331–344.

8 F. Bird, A. Clarke, P. Davies and E. Surkovic, *Ammonia: Zero-Carbon Fertiliser, Fuel and Energy Store (Policy Briefing)*, The Royal Society, London, UK, 2020.

9 J. G. Chen, R. M. Crooks, L. C. Seefeldt, K. L. Bren, R. M. Bullock, M. Y. Darensbourg, P. L. Holland, B. Hoffman, M. J. Janik, A. K. Jones, M. G. Kanatzidis, P. King, K. M. Lancaster, S. V. Lymar, P. Pfromm, W. F. Schneider and R. R. Schrock, *Science*, 2018, **360**, eaar6611.

10 S. Chatterjee, R. K. Parsapur and K.-W. Huang, *ACS Energy Lett.*, 2021, **6**, 4390–4394.

11 R. F. Service, *Science*, 2018, **361**, 120–123.

12 S. Bouckaert, A. F. Pales, C. McGlade, U. Remme, B. Wanner, L. Varro, D. D'Ambrosio and T. Spencer, *Net Zero by 2050: A Roadmap for the Global Energy Sector*, International Energy Agency, Paris, France, 2021.

13 L. Hu, Z. Xing and X. Feng, *ACS Energy Lett.*, 2020, **5**, 430–436.

14 D. Liu, M. Chen, X. Du, H. Ai, K. H. Lo, S. Wang, S. Chen, G. Xing, X. Wang and H. Pan, *Adv. Funct. Mater.*, 2021, **31**, 2008983.

15 M. Wang, M. A. Khan, I. Mohsin, J. Wicks, A. H. Ip, K. Z. Sumon, C.-T. Dinh, E. H. Sargent, I. D. Gates and M. G. Kibria, *Energy Environ. Sci.*, 2021, **14**, 2535–2548.

16 D. R. MacFarlane, P. V. Cherepanov, J. Choi, B. H. R. Suryanto, R. Y. Hodgetts, J. M. Bakker, F. M. Ferrero Vallana and A. N. Simonov, *Joule*, 2020, **4**, 1186–1205.

17 S. Y. Park, Y. J. Jang and D. H. Youn, *Catalysts*, 2023, **13**, 639.

18 Y. Abghoui, A. L. Garden, V. F. Hlynsson, S. Björgvinsdóttir, H. Ólafsdóttir and E. Skúlason, *Phys. Chem. Chem. Phys.*, 2015, **17**, 4909–4918.

19 Y. Abghoui, A. L. Garden, J. G. Howalt, T. Vegge and E. Skúlason, *ACS Catal.*, 2016, **6**, 635–646.

20 Y. Abghoui and E. Skúlasson, *Procedia Comput. Sci.*, 2015, **51**, 1897–1906.

21 Y. Abghoui and E. Skúlason, *Catal. Today*, 2016, **286**, 69–77.

22 Y. Abghoui and E. Skúlason, *J. Phys. Chem. C*, 2017, **121**, 6141–6151.

23 X. Zhang, R.-M. Kong, H. Du, L. Xia and F. Qu, *ChemComm*, 2018, **54**, 5323–5325.

24 H.-L. Du, T. R. Gengenbach, R. Hodgetts, D. R. MacFarlane and A. N. Simonov, *ACS Sustain. Chem. Eng.*, 2019, **7**, 6839–6850.

25 X. Ren, G. Cui, L. Chen, F. Xie, Q. Wei, Z. Tian and X. Sun, *ChemComm*, 2018, **54**, 8474–8477.

26 B. Hu, M. Hu, L. Seefeldt and T. L. Liu, *ACS Energy Lett.*, 2019, **4**, 1053–1054.

27 Y. Abghoui and E. Skúlason, *Catal. Today*, 2017, **286**, 78–84.

28 D. H. Youn, G. Bae, S. Han, J. Y. Kim, J.-W. Jang, H. Park, S. H. Choi and J. S. Lee, *J. Mater. Chem. A*, 2013, **1**, 8007–8015.

29 Y. Wang, W. Zhou, R. Jia, Y. Yu and B. Zhang, *Angew. Chem., Int. Ed.*, 2020, **59**, 5350–5354.

30 X. Yang, J. Nash, J. Anibal, M. Dunwell, S. Kattel, E. Stavitski, K. Attenkofer, J. G. Chen, Y. Yan and B. Xu, *J. Am. Chem. Soc.*, 2018, **140**, 13387–13391.

31 P. Song, H. Wang, L. Kang, B. Ran, H. Song and R. Wang, *Chem. Commun.*, 2019, **55**, 687–690.

32 H. E. Kim, J. Kim, E. C. Ra, H. Zhang, Y. J. Jang and J. S. Lee, *Angew. Chem., Int. Ed.*, 2022, **61**, e202204117.

33 Y. J. Jang and K.-S. Choi, *J. Mater. Chem. A*, 2020, **8**, 13842–13851.

34 W. Guo, Z. Liang, Y. Tang, K. Cai, T. Qiu, Y. Wu, K. Zhang, S. Gao and R. Zou, *J. Mater. Chem. A*, 2021, **9**, 8568–8575.

35 G. Jouve, C. Séverac and S. Cantacuzène, *Thin Solid Films*, 1996, **287**, 146–153.

36 B. Kościelska and A. Winiarski, *J. Non-Cryst. Solids*, 2008, **354**, 4349–4353.

37 H. Cui, G. Zhu, X. Liu, F. Liu, Y. Xie, C. Yang, T. Lin, H. Gu and F. Huang, *Adv. Sci.*, 2015, **2**, 1500126.

38 T. Zhao, S. Shen, X. Liu, Y. Guo, C.-W. Pao, J.-L. Chen and Y. Wang, *Catal. Sci. Technol.*, 2019, **9**, 4002–4009.

39 S. Leith, M. Vogel, X. Jiang, E. Seiler and R. Ries, 2019, 947–951.

40 J. Alfonso, J. Buitrago, J. Torres, J. Marco and B. Santos, *J. Mater. Sci.*, 2010, **45**, 5528–5533.

41 L. Zhang, X. Ji, X. Ren, Y. Luo, X. Shi, A. M. Asiri, B. Zheng and X. Sun, *ACS Sustain. Chem. Eng.*, 2018, **6**, 9550–9554.

42 S. Kang, J. Wang, S. Zhang, C. Zhao, G. Wang, W. Cai and H. Zhang, *Electrochem. Commun.*, 2019, **100**, 90–95.

43 R. Manjunatha, A. Karajić, H. Teller, K. Nicoara and A. Schechter, *ChemCatChem*, 2020, **12**, 438–443.